Small-Angle X-Ray Scattering from Lipid Bilayers Is Well Described by Modified Caillé Theory but Not by Paracrystalline Theory

Ruitian Zhang,* Stephanie Tristram-Nagle,‡ Wenjun Sun,* R. L. Headrick,§ T. C. Irving,¶ Robert M. Suter,* and John F. Nagle*,‡

*Department of Physics and ‡Department of Biological Sciences, Carnegie Mellon University, Pittsburgh, Pennsylvania 15213, and §Cornell High Energy Synchrotron Source ¶MacCHESS, Division of Biochemistry, Molecular and Cell Biology, Ithaca, New York 14853 USA

ABSTRACT X-ray scattering data at high instrumental resolution are reported for multilamellar vesicles of L_α phase lipid bilayers of 1,2-dipalmitoyl-*sn*-glycero-3-phosphatidylcholine at 50°C under varying osmotic pressure. The data are fitted to two theories that account for noncrystalline disorder, paracrystalline theory (PT) and modified Caillé theory (MCT). The MCT provides good fits to the data, much better than the PT fits. The particularly important characteristic of MCT is the long power law tails in the scattering. PT fits (as well as ordinary integration with no attempt to account for the noncrystalline disorder) increasingly underestimate this scattering intensity as the order h increases, thereby underestimating the form factors used to obtain electron density profiles.

INTRODUCTION

It is well known that lipid bilayers have different thicknesses and different areas per lipid molecule for different lipids (Rand and Parsegian, 1989; Thurmond et al., 1991; McIntosh and Simon, 1986a,b). However, the actual values of these quantities are rather poorly determined (Tristram-Nagle et al., 1993; Nagle, 1993), so that the differences between different lipid bilayer systems are comparable to the experimental uncertainty, especially for the biologically relevant fluid (L_α) phase.

One source of uncertainty in structural determinations of lipid bilayers is endogenous; namely, these are not crystalline systems, so the methods of crystallography cannot necessarily be expected to apply. Nor can a realistic goal be to obtain atomic structure at angstrom resolution, as the systems are disordered and fluctuating. The fluctuations are described by various kinds of correlation functions, some of which are more fluid-like than crystal-like (Wiener and White, 1991). Indeed, the most popular sample preparation for structure determination consists of multilamellar vesicles (MLVs) that are best characterized as liquid crystals.

Even though the liquid crystal nature of MLV samples of lipid bilayers is well known, the occurrence of very sharp, well separated, small-angle scattering peaks means that there are well defined D-spacings in MLVs. This, in turn, has motivated the determination of low resolution structure along the bilayer normal by measuring the intensities of the scattering peaks and applying the usual Lorentz correction to obtain the square of the form factors (Torbet and Wilkins, 1976; Worthington and Khare, 1978; Franks and Lieb, 1979; McIntosh and Simon, 1986a,b; Kim et al., 1987; Wiener et al., 1989). After applying various methods to obtain the phases, electron density profiles have then been obtained.

The standard procedure in the preceding paragraph does not take into account the liquid crystalline nature of MLVs. The analysis assumes that each scattering peak is a Bragg peak, with perhaps some broadening as a result of finite size of the scattering domains. However, there are two theories that both show that disorder removes scattering intensity from the central peaks and pushes it into the troughs between the peaks where it merges with the background and cannot be accurately measured. Most importantly, this effect becomes progressively larger as the order h of the scattering peaks increases. This is a major factor accounting for the absence of higher order peaks. Even for those peaks that one can observe, measuring only the intensities under the central peaks systematically underestimates the higher order form factors, thereby degrading the electron density profile.

One theory that allows the above artifact to be corrected is paracrystalline theory (PT) (Hosemann and Bagchi, 1962; Guinier, 1963); this theory has been applied to multilamellar arrays of retinal rod membranes (Schwartz et al., 1975; Worthington, 1989) and nerve myelin (Blaurock and Nelander, 1976). Another theory is the Caillé theory (CT) (Caillé, 1972), recently modified (MCT) (Zhang et al., 1994); this theory has been applied to multilamellar arrays of lipid bilayers and to various liquid crystal systems (Roux and Safinya, 1988; Zhang et al., 1995). Although these two theories are both based on the general notion of disorder, the details of the theories are quite different and, most importantly, the predicted corrections are different, as we show in the theory section of this paper. The primary goals of this paper, then, are to determine whether either of these two theories describes scattering from lipid bilayers and, if so, which one is better. If this is successful, appropriate correc-

Received for publication 19 June 1995 and in final form 14 September 1995.

Address reprint requests to Dr. John F. Nagle, Department of Physics, Carnegie Mellon University, Pittsburgh, PA 15213. Tel.: 412-268-2764; Fax: 412-681-0648; E-mail: jn12@andrew.cmu.ed.

0006-3495/96/01/349/09 $2.00

tions to the form factors can be made in subsequent work to obtain better electron density profiles.

This kind of work requires that the experimental shapes of the peaks and their tails be well resolved. Fortunately, even though the peaks are very sharp, it is possible to resolve their shapes (not just their separations, which is easy) using high instrumental resolution diffraction (half-width at half-maximum (HWHM) in δq of 0.0001 $Å^{-1}$). As very few photons are scattered by lipid bilayers in such small angular ranges (~0.001°), we also use a synchrotron source. This combination enables us to achieve our primary goals.

THEORY

Paracrystalline theory (PT)

The simplest model for disorder in multilamellar vesicles is to suppose that the local spacing D between each neighboring pair of bilayers is a random variable with a mean value of $\bar{D}$ and mean square fluctuations defined by

$$\Delta^2 \equiv \langle (D - \bar{D})^2 \rangle. \quad (1)$$

PT assumes that these nearest neighbor fluctuations are independent for each pair of neighboring bilayers in the multilamellar array. Therefore, the mean square fluctuation in the distance between bilayers separated by $n - 1$ intervening bilayers is given by

$$\Delta_n^2 = n\Delta^2. \quad (2)$$

The divergence of Δ_n for large n contrasts strongly with truly crystalline systems for which the mean square fluctuations remain bounded at large distances. It should be emphasized that this is a stochastic model with no Hamiltonian dynamics. It is also assumed that each bilayer in the array remains flat, with no bending undulations, as shown in Fig. 1, thus treating multilamellar arrays as pure one-dimensional systems, as emphasized by Guinier (1963). Although our results will indicate that PT is not appropriate for multilamellar arrays of lipid bilayers, it is worth noting that such a theory may be appropriate for one-dimensional systems, such as helices (Worthington and Elliott, 1989) and that it is also possible that multilamellar arrays of nerve myelin (Blaurock and Nelander, 1976) or retinal rods (Schwartz et al., 1975) may be adequately described by disorder of the paracrystalline kind.

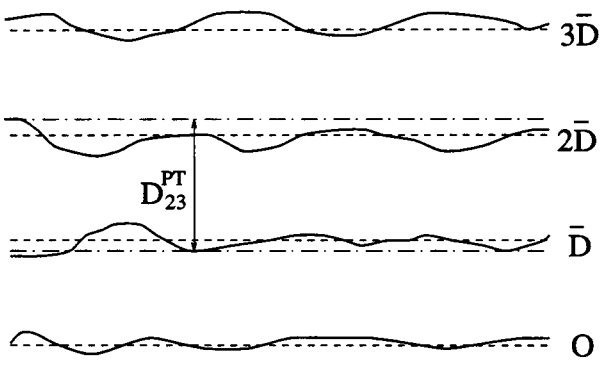

FIGURE 1 The dashed lines show the centers of four bilayers stacked in a perfectly crystalline array. The dot-dash lines show a snapshot of paracrystalline fluctuations in which the second and third bilayers are displaced with a resulting local D-spacing D_{23}^{PT}. The solid lines show a snapshot of the fluctuations of the Caillé theory that also involve undulations.

It was shown by Guinier (1963) that, when the mean square fluctuations in Eq. 2 are incorporated into the phase factors for scattering between pairs of bilayers, the basic scattering formula for the structure factor $S(q)$ for N oriented bilayers (domain size $L = ND$) becomes

$$S(q) = N + 2\sum_{n=1}^{N-1} (N - n)\cos(qnD)e^{-n\Delta^2q^2/2}, \quad (3)$$

where the average spacing $\bar{D}$ is now written just as D, and q is q_z. To avoid terminological confusion, it should be emphasized that the structure factor in Eq. 3 gives only the scattering from infinitely thin bilayers. (For comparison, if the sample consisted of large crystals, $S(q)$ would be given by delta functions of equal amplitude at each Bragg peak.) The actual scattering $I(q)$ is given (Zhang et al., 1994) by

$$I(q) = S(q)|F(q)|^2/q^2, \quad (4)$$

where the factor of q^{-2} is the Lorentz factor for unoriented powder samples and $F(q)$ is the form factor that is related to the electron density profile $\rho(z)$ by

$$F(q) = \int_{-D/2}^{D/2} \rho(z)\cos(qz)dz. \quad (5)$$

For smectic liquid crystals, Eq. 3 allows for finite size effects by taking finite values of N. As it is unlikely that all domains in a sample will have precisely the same number of bilayers, it is also appropriate to consider a distribution of N or L values. We will assume the distribution function

$$P(L) \propto e^{-(L-L_0)^2/2\sigma_L^2}, \quad (6)$$

which is essentially a Gaussian except that $P(L) = 0$ for $L < 0$. The mean values of this distribution will be designated $\bar{L}$ (which is generally not equal to L_0) and the mean square fluctuation (distribution) in L will be designated σ_L.

Fig. 2 shows the first five scattering peaks from PT plotted versus q/q_1 for particular values of the parameters, Δ, $\bar{L}$, and σ_L, which are close to those that emerge from our data. For higher orders (not shown) the peaks continue to decrease in height and diffuse scattering between the peaks increases until $S(q)$ approaches a constant. (Even the first five peaks for $S(q)$ decrease rapidly in height with increasing h and that is why $qS(q)$ is plotted in Fig. 2.) Fig. 3 shows the first three PT peaks at higher angular resolution for a

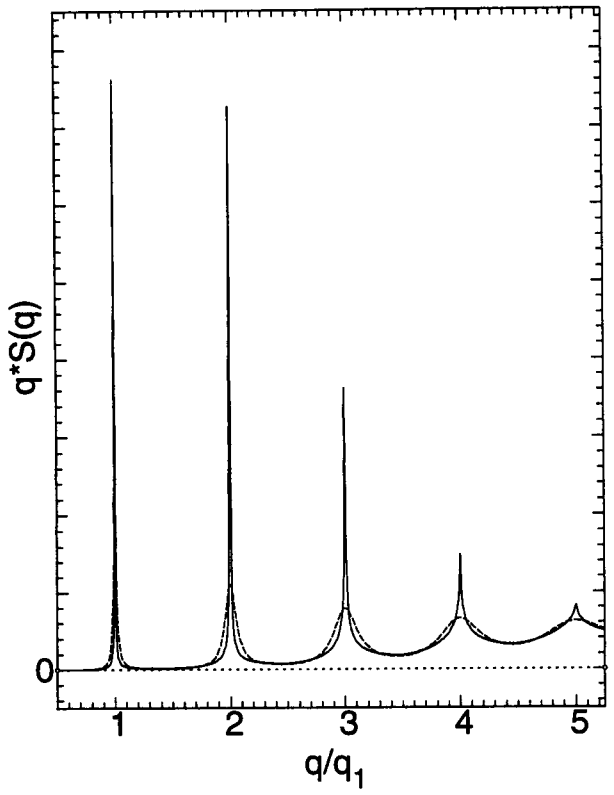

FIGURE 2 The structure factor $S(q)$ times q for PT (*dashed lines*) and MCT (*solid lines*) versus q/q_1 for Δ = 4.0 Å, $\bar{L}$ = 4270 Å, and σ_L = 3600 Å.

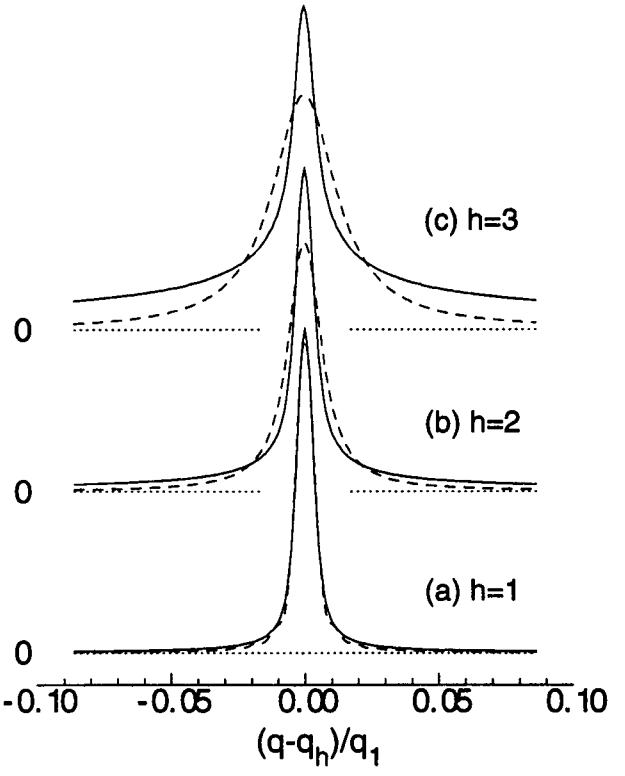

FIGURE 3 The solid lines show typical $S(q)$ for MCT for the first three peaks, (*a*) h = 1, (*b*) h = 2, and (*c*) h = 3, for D = 60 Å and $q_1 = 2\pi/D$. The peak heights are normalized to unity and the peak maxima are shifted to zero for comparison of peak shapes for different orders h. Values of the parameters are η_1 = 0.050 (Δ_c = 4.0 Å), $\bar{L}$ = 4270 Å, and σ_L = 3600 Å. The dashed lines show the best fit to the solid curves using PT which yields Δ_p = 1.2 Å, $\bar{L}$ = 8440 Å, and σ_L = 1560 Å. The dotted lines show the zero levels for each order.

smaller value of Δ. The peaks grow broader proportional to h^2 (Schwartz et al., 1975) and the tails of the peaks are essentially Lorentzian with

$$S(q) \sim (q - q_h)^{-2}. \tag{7}$$

Modified Caillé Theory (MCT)

Although PT is a reasonable first attempt to deal with disorder in multilamellar arrays, one might prefer a scattering theory that allows for bending of the bilayers in addition to fluctuations in the mean spacings between bilayers as well as one that is based on energetics of the fluctuations rather than just an arbitrary stochastic assumption. Such a theory was originally presented by Caillé (1972) who built upon the thermodynamic theory of DeGennes (1974) for smectic liquid crystals. This theory arrives at some quite different conclusions than PT. For example, the mean square fluctuations Δ_n^2 in the multilayered sample diverge logarithmically with n instead of linearly as in Eq. 2. This has strong consequences for scattering. In particular, for powder samples (Roux and Safinya, 1988; Zhang et al., 1994), the tails of the scattering peaks decay according to the power law behavior

$$S(q) \sim (q - q_h)^{-1+\eta}. \tag{8}$$

The parameter η involves the bending modulus K of lipid bilayers and the bulk modulus B for compression

$$\eta = \frac{q^2 kT}{8\pi\sqrt{KB}}. \tag{9}$$

Because η varies as q^2 and because each peak is well separated from other peaks, it is appropriate to report just η_1, which is defined to be the value of η at q_1 for the h = 1 first order peak, recognizing that η near the hth order peak is given by

$$\eta_h = \eta_1 h^2. \tag{10}$$

Detailed fitting using classical Caillé and domain size theory has given quite good visual fits to scattering peaks from a variety of smectic liquid crystalline systems (Roux and Safinya, 1988).

We have modified the Caillé theory in a recent theoretical paper (Zhang et al., 1994). Our modifications did not affect any of the qualitative results in the preceding paragraph, but they were necessary for obtaining better quantitative fits to data and particularly for extracting the correct form factors to be used for obtaining electron density profiles. The

present paper will use Eqs. 80 and 82 in Zhang et al. (1994), which will be described as MCT.

Despite the much richer and more realistic model for multilamellar arrays, MCT has effectively the same number of parameters for fitting scattering peaks as PT. The parameter η_1 in MCT is basically a disorder parameter much like Δ in PT. Numerical values of η_1 also translate to mean square nearest neighbor distance fluctuations Δ_c^2 given by Eq. 1. The derivation requires use of the pair correlation functions (Zhang et al., 1994) and yields

$$\Delta_c^2 = 0.087\eta_1 D^2. \quad (11)$$

The other two basic parameters in both MCT and in PT are the mean size of domains $\bar{L}$ and the root mean square distribution σ_L of domain size in Eq. 6.

Comparison of PT and MCT

Before turning to experimental data, it is useful to compare the two theories to see how their predictions for the shapes of the scattering peaks differ. Fig. 2 compares the MCT and PT curves for the same values of the parameters that are typical of those that fit some of our experimental data (*vide infra*). Both theories predict substantial increases in the diffuse or tail scattering between the peaks, but the PT peaks broaden and disappear much more rapidly whereas the MCT peaks retain a sharper top.

The more interesting way to compare the two theories is shown in Fig. 3, which shows the same first three MCT peaks in Fig. 2. However, the parameters for the PT peaks have now been chosen to provide the best fits to the MCT curves. The fits are performed simultaneously for all three peaks shown in both figures, with, of course, the same sample parameters for PT for each peak. It should be emphasized that, when we start with peaks calculated from PT and fit them with MCT peaks, the same differences are observed, so the comparison is not biased toward either theory. Fig. 3 emphasizes that the central parts of the MCT peaks remain sharp and the tails increase substantially with increasing order h. For PT, in contrast, the central peaks broaden much more and the tails grow much more slowly with increasing h. Therefore, PT predicts larger values of the intensity near half-maximal intensity and smaller values of the scattering near maximal intensity as well as in the tails.

It is important to consider how the aforementioned differences affect the determination of the form factors in Eq. 4. The total integrated area under the peaks in Fig. 3 is different for MCT and for PT and the ratio $R^2(h)$ of the MCT area to the PT area gives the ratio of the square of the form factors $F(h)$. For the first order we set $R(1) = 1$ because our x-ray measurements do not give absolute intensities. Then, from the fit in Fig. 3 we obtain $R(2) = 1.10$ and $R(3) = 1.38$. This shows that PT fits to the data progressively underestimate higher order form factors used for obtaining electron density profiles if the sample obeys the dynamics of MCT; this is primarily because of the loss of the intensity in the long power law tails of the Caillé theory. Similarly, MCT fits to data overestimate higher order form factors if PT were correct. Therefore, determining the appropriate theory of disorder and fluctuations affects the determination of average bilayer structure through electron density profiles. Deciding which is the appropriate theory, in turn, requires high precision experimental data to resolve the peak shapes.

EXPERIMENTAL

Samples

1,2-Dipalmitoyl-*sn*-glycero-3-phosphatidylcholine (DPPC; lot 160PC-198) was purchased from Avanti Polar Lipids (Alabaster, AL), and no lysolecithin was found by thin layer chromatography. Polyvinylpyrrolidone (PVP; mw = 40,000) was purchased from Sigma Chemical Co. (St. Louis, MO) and dried in a 70°C oven overnight. PVP solutions from 5 to 45% (w:w) were prepared by mixing dried PVP with distilled, deionized water. PVP solutions were added to dried DPPC in a 3:1 (for 30% PVP and below) or 4:1 (for 35% PVP and above) weight ratio. The samples were cycled in 5-min intervals between 70°C and 5°C three times with vortexing, then held at 50°C for 3–4 hours, and finally allowed to equilibrate overnight at room temperature. The samples were loaded into carefully cleaned thin-walled 1.0- or 1.5-mm flint glass x-ray capillaries (Charles Supper Co., Cambridge, MA) flame-sealed at one end. The capillaries were centrifuged for 10 min at $1100 \times g$ to remove air bubbles. At PVP concentrations of 30% and above, the lipid dispersions centrifuged up instead of down at 0°C. The capillaries were then flame-sealed at the other end and loaded into cassettes with 14 slots/cassette. Both ends of the capillaries were embedded in slabs of silicone sealer to insure against dehydration. These cassettes fit directly into a custom cassette holder that was contained in a cylindrical aluminum sample chamber with two 1.5-μm-thick mylar windows for entry and exit of x-rays. Temperature was controlled by a Lake Shore Cryotronics Model DRC-91C temperature controller (Westerville, OH), which responded to a 1000-ohm platinum resistance thermometer in the center of the sample cassette (Rosemount, Eagen, MN). Temperature stability was ± 0.02°C. The chamber was attached to X-Y-Z motorized translations to move the samples in the x-ray beam.

X-ray intensity measurements

High instrumental resolution x-ray scattering experiments were performed at the Cornell High Energy Synchrotron Source (CHESS) on the F3 station. A double-bounce Si monochromator was calibrated to 1.2147-Å x-rays, the scattering angles were selected by Bragg diffraction from the (111) face of a Si analyzer crystal, and the intensity was measured by a NaI scintillation detector. A diagram of the

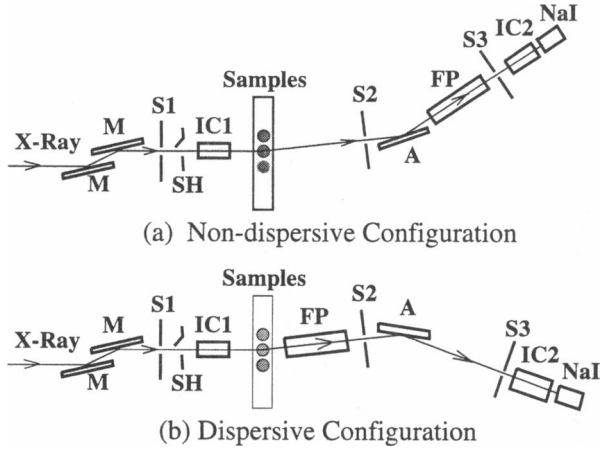

FIGURE 4 High resolution x-ray configurations M, Si monochromator crystal; S1, sample slits; SH, automatic shutter; IC, ion chamber detector; S2, scatter slits; A, Si analyzer crystal; FP, flight path (filled with N_2 gas); S3, detector slits; NaI, scintillator detector. (*a*) Nondispersive configuration. (*b*) Dispersive configuration.

experimental set-up is shown in Fig. 4. The beam size, as defined by the S1 slit, was approximately 1.0 mm high and 1.5 mm wide. The beam flux on the sample was approximately 2×10^9 photons/s/mm^2.

The detector IC1 was used to monitor the incoming x-ray flux. The automatic shutter SH was open only during counting to minimize unnecessary exposure of samples to the x-ray beam. The ion chamber IC2 was used to detect the main beam. The NaI scintillator detector was used to detect the much weaker diffracted beam.

The longitudinal resolution (see Als-Nielsen et al., 1980 for definitions used in this paragraph) is determined by the combination of monochromator and analyzer crystals. Half of our data was taken in the nondispersive configuration (Fig. 4 *a*), which had a longitudinal resolution with HWHM of 1.0×10^{-4} Å^{-1}. The other half of our data was obtained in the dispersive configuration, which had longitudinal resolution of 3.3×10^{-4} Å^{-1} (HWHM). The out-of-scattering-plane resolution is mainly determined by the horizontal angular acceptance of the slits S1 and S3 and was 6×10^{-3} Å^{-1}. The relatively poorer out-of-plane resolution leads to a small amount of slit smearing, but this is easily accommodated in the data analysis. (Incidentally, it may be noted that the term resolution in this and most physics x-ray scattering studies refers to instrumental resolution in q-space, which should not be confused with the direct space resolution of a structure determination.)

It may be useful to emphasize that the above experimental configuration, which uses an analyzer crystal, is intrinsically different from position-sensitive detection, including film. These latter methods incur geometric artifacts involving the sample size and the length of the path for the scattered radiation that broaden peaks with increasing h as was carefully analyzed by Franks and Lieb (1979), but such artifacts are absent in our configuration. Also, to achieve the resolution in our configuration with even the best area or position-sensitive detector, geometric artifacts would require scattering path lengths of 30 m for a beam that is 1 mm in height.

With this experimental configuration, radiation damage, indicated by systematic changes in the shape and position of the first order peak, did not become apparent until after half an hour of exposure time in the nondispersive configuration. As a precaution, the maximal exposure time for typical data was 15 min after which the capillaries were translated to expose a fresh section of the sample. Also, thin layer chromatography on exposed samples indicated that only 0–2% lysolecithin formed per capillary, and the amount of lipid degradation was not simply proportional to the exposure time or to the time the sample remained near 50°C. Normalization of the scattering from two different exposures of the same capillary was obtained by comparison of brief scans of the intense first order peaks. Experimental protocol for the dispersive mode employed single scans through the peaks with equally spaced angular increments. In the nondispersive mode, several scans were made through each peak with different angular increments for each scan.

The weak background scattering from capillaries containing air, pure water, 25% PVP solution, and 50% PVP solution was measured using long counting times. Estimated uncertainties in background scattering are roughly 10%, and error bars for the background-subtracted data include the uncertainties from background determination. The angular range of the reported data for the tails of the peaks was restricted so that the average intensity was at least twice as great as the background. Also, the ratio of the maximal peak signal to the background was roughly 200 for the first order peak and roughly 50 for the second order peak.

Data fitting

Nonlinear least squares fitting of the theoretical curves to the data was performed using the LMDER subroutine from the MINPACK library (Garbow et al., 1980). Starting values of the parameters were estimated from experience and tens of different starting values were tried to reduce the possibility of getting caught in local minima. The basic parameters in the fit were η_1, L, σ_L, and the amplitude for each peak in the simultaneous fit to all peaks with the constraint in Eq. 10. Because of small (less than 1%) mechanical hysteresis in the 2θ arm at CHESS that we carefully documented, some of the peak position values q_h do not index perfectly and were therefore made parameters. Also, for some of our earlier data the out-of-plane resolution σ_x was not measured carefully and was allowed to be a parameter, although its range was consistent within 10% with our estimates from slit widths. Uncertainties in parameter values were estimated from the inverse curvature matrix for the residual sum of squares.

RESULTS

We have obtained x-ray scattering data at high instrumental resolution for the L_α (fluid, chain-melted) phase of DPPC at 50°C for samples exhibiting a wide variety of D-spacings, as summarized in Table 1. Smaller D-spacings occurred when higher osmotic pressure was applied by increasing the concentration of PVP. The maximal number h_{max} of observable small-angle lamellar scattering peaks increased as D decreased. Incidentally, we have consistently found that the D-spacing of fully hydrated DPPC (with 0% PVP) varies noticeably from sample to sample. The first two samples in Table 1 give the maximal range that we have observed, although it may be noted that Shipley's group (Janiak et al., 1976) has observed D-spacings as low as 60.0 Å.

Fig. 5 shows the scattering data for the DPPC sample with 0% PVP and D = 64.5 Å. Although these data were taken with the wider longitudinal resolution using the dispersive detector set-up, the peak shapes are well resolved. The PT fit to the first order peak appears visually to be nearly as good as the MCT fit, but the MCT fit to the second order peak is clearly superior. As can be seen in Table 1, the ratio of the χ^2 for the two theories is 3.6, indicating that MCT is far superior to PT.

Fig. 6 shows the scattering for the other 0% PVP sample with D = 67.2 Å. These data were taken with our highest resolution. The scattering for $q - q_1 > 0.003$ Å^{-1} appears to be anomalously high and erratic; these data points are not fit well by either theory, which accounts for the relatively large values of χ^2. Nevertheless, the ratio of χ^2 for the two theories strongly supports the conclusion that MCT is better than PT.

Fig. 7 shows scattering data for the 25% PVP sample with D = 58.2 Å. Again, although there is little difference in the fits to the first order peak, MCT clearly fits both higher order peaks better than PT. Data (not shown) for the other three samples confirms this general conclusion. We have also analyzed much additional data from DPPC using only MCT with similar results that will be reported in a subsequent publication. MCT fits to less extensive data from dimyristoylphosphatidylcholine (DMPC) have previously been shown by Zhang et al. (1995); these latter fits gave smaller χ^2 values near 1.4 by relaxing the constraint in Eq. 10.

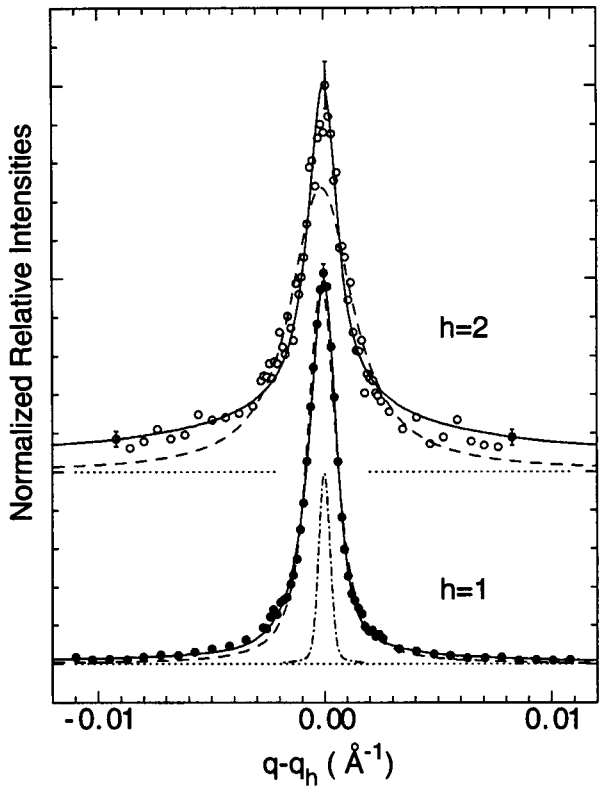

FIGURE 5 The solid lines show MCT fit to DPPC data with 0% PVP and D = 64.5 Å. The peak heights are normalized to unity and the peak maxima are shifted to zero for comparison of peak shapes for different orders h. The dashed lines show the best fit using the PT. Parameter values are listed in Table 1. The dash-dot line shows the resolution function. The dotted lines show the background-subtracted zero levels for each order. For clarity, counting statistics error bars are shown only for three data points at the ends and middle of each peak.

The best fits to the data yield the values of the parameters reported in Table 1. As expected, the values of η_l, Δ_c, and Δ_p decrease monotonically with decreasing D as fluctuations in the multilamellar vesicles are suppressed by increased osmotic pressure. Table 1 shows that the root mean square fluctuations in nearest neighbor distances, which are given by Δ_c for MCT (from Eq. 11) and by Δ_p from the PT fit, are predicted to be larger by MCT than by PT, by a factor that varies from approximately 2 to nearly 4 as D

TABLE 1 Results of fitting MCT (c subscripts) and PT (p subscripts) to six samples of DPPC at 50°C with varying D spacings due to varying concentrations of PVP

D (Å)	% PVP	h_{max}	δq_{res} (Å^{-1})	χ^2_c	χ^2_p	η_l	Δ_c (Å)	Δ_p (Å)	$\bar{L}_c$ (Å)	$\bar{L}_p$ (Å)	σ_{Lc} (Å)	σ_{Lp} (Å)	R_{max}
67.2	0	2	0.0001	2.81	5.62	0.184	8.5	4.1	1930	2890	1450	3570	1.24
64.5	0	2	0.00033	1.81	6.52	0.097	5.9	2.1	3750	3540	4250	4440	1.29
62.5	5	2	0.0001	1.60	4.32	0.074	5.0	1.6	4180	8450	5210	10560	1.27
60.4	15	3	0.0001	2.06	3.37	0.058	4.3	1.3	5270	9610	6020	10400	1.41
58.2	25	3	0.00033	1.32	3.17	0.046	3.7	1.1	7040	13290	8610	6520	1.49
55.06	40	4	0.00033	1.85	3.27	0.033	3.0	0.83	16790	15490	2530	10320	1.82

Δ is the root mean square fluctuation in nearest neighbor membrane distances, η_l is defined in Eq. 9, and $\bar{L}$ and σ_L are defined in Eq. 6. R_{max} is the ratio of form factors at h_{max}, $F_c(h_{max})/F_p(h_{max})$.

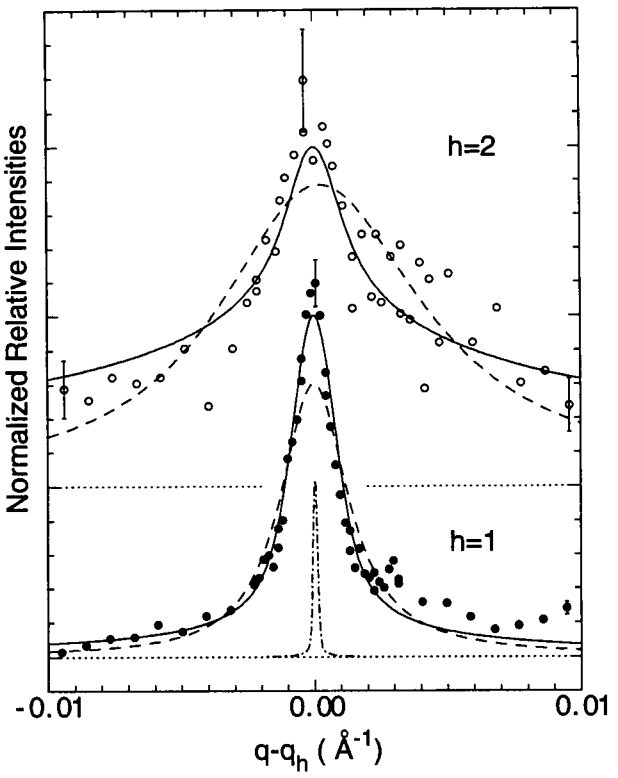

FIGURE 6 0% PVP sample data; D = 67.2 Å. Solid lines, MCT fits; dashed lines, PT fits; dash-dot lines, resolution function; dotted lines, background-subtracted zero levels for each order. Parameter values are listed in Table 1. Error bars are shown for three data points for each peak.

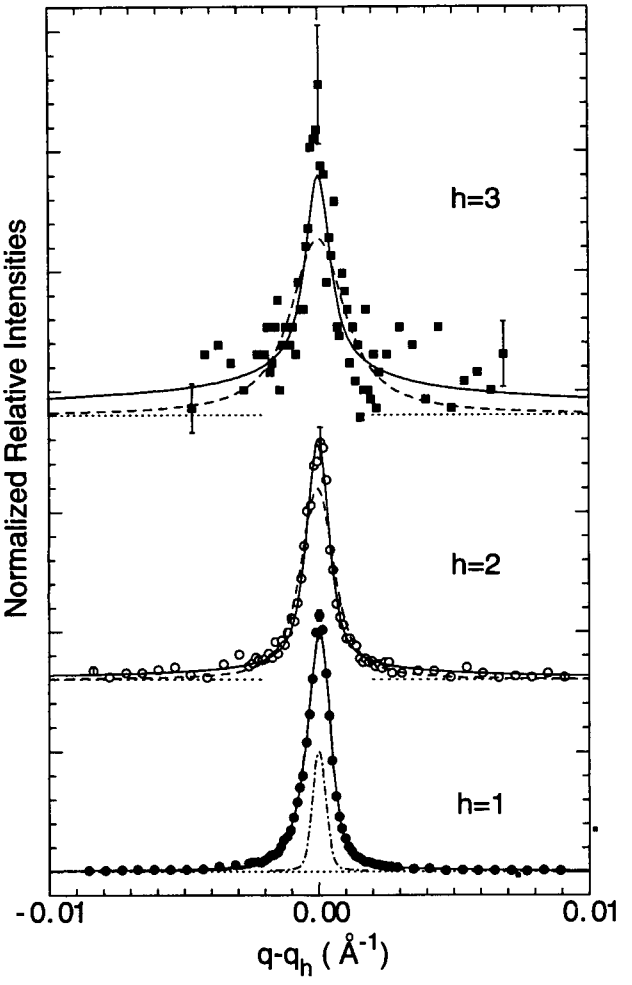

FIGURE 7 25% PVP sample data; D = 58.2 Å. Solid lines, MCT fits; dashed lines, PT fits; dash-dot lines, resolution function; dotted lines, background subtracted zero levels for each order. Parameter values are listed in Table 1. Error bars are shown for three data points for each peak.

decreases. The probable uncertainties in the parameters η_l and Δ are quite small, of the order 1%. The mean domain sizes $\bar{L}$ are quite large for both theories, corresponding to average number N of bilayers per domain from 30 to 300. As the values of σ_L are comparable to the values of $\bar{L}$ for both theories, the domain size distribution is quite broad.

The final column in Table 1 indicates how the form factors that arise from fits to the data using MCT and PT differ. Specifically, the form factors $F(1)$ for the first order peaks are normalized to unity for the fits from both theories. The fits to the peak shapes yield $S(q)$ shapes with amplitudes that give $F(h)$ according to Eq. 4. Finally, for the highest order peak, h_{max}, the ratio, $R_{max} = F_c(h_{max})/F_p(h_{max})$, of the MCT form factor to the PT form factor is reported in Table 1.

Finally, it may be of interest to see how our modifications to the Caillé theory affect fits to the data compared with the unmodified Caillé theory that was used earlier by Roux and Safinya (1988). Previous authors did not report χ^2 values and it is difficult in any case to compare different experiments directly. However, we have performed fits to some of our data using the unmodified Caillé theory, as shown in Fig. 8. The $\chi^2 = 5.74$ for the unmodified Caillé theory is much larger than the $\chi^2 = 1.81$ for the modified theory. The unmodified theory does a good job fitting the tails; the primary reason for the larger χ^2 is the difficulty in fitting the sharp first order peak, which is primarily because of the classical finite size factor, which is an artificial approximation (Zhang et al., 1994). It is interesting to compare the unmodified Caillé theory to PT, which fits the $h = 1$ peak better (Fig. 5) but has trouble with the h = 2 peak for which the tails are larger.

DISCUSSION

The MCT fits to our x-ray scattering data taken at high resolution are quite good, as seen visually by the fits in Figs. 5–7. Although the reduced χ^2 values in Table 1 are systematically greater than 1, this is to be expected because the only errors used in computing the χ^2 were the counting statistics; accounting for other errors, such as small random fluctuations in the 2θ angles, would reduce the χ^2 values. Therefore, the modified Caillé theory appears to be appropriate for lipid bilayers. By comparison, the PT fits are clearly worse than MCT fits, with much larger χ^2 values

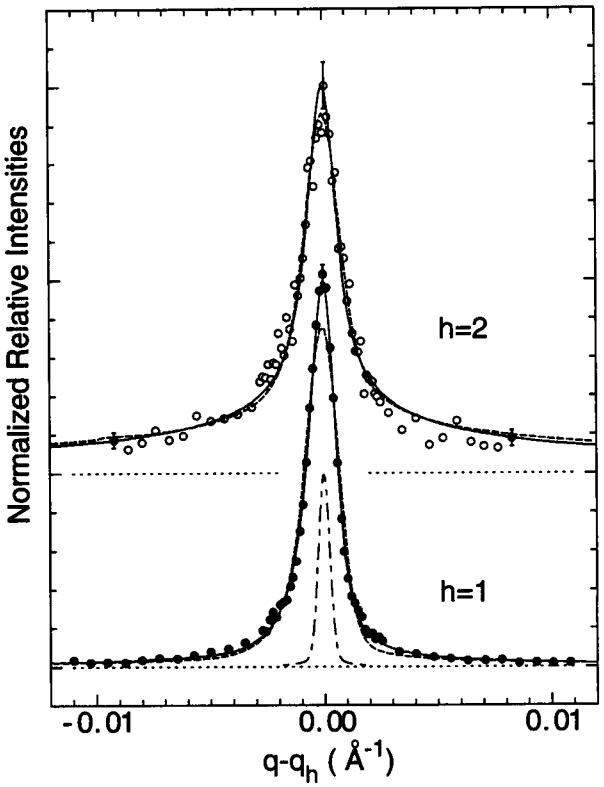

FIGURE 8 Same sample as in Fig. 5. Solid lines, MCT fits; dashed lines, ordinary Caillé theory fits.

and with systematic residuals in the tails and the central peaks that are not present in the MCT fits.

Theoretically, it is not surprising that MCT is more appropriate than PT for L_α phase multilamellar vesicles. Whereas PT attempts to guess the nature of the fluctuations by imposing a stochastic assumption on the correlations between bilayers, MCT utilizes a reasonable free energy to describe the fluctuations. Furthermore, MCT allows for both undulation fluctuations as well as compressional fluctuations; PT considers only the latter.

PT fits consistently underestimate the central peak and the tails and overestimate the shoulders. PT tries to compensate for the sharp central peak by predicting a domain size larger than that given by MCT and by underestimating the size of the fluctuations of the distance between nearest neighboring membranes (see Table 1 and Fig. 3). As will be shown in subsequent work, the larger root mean square fluctuation in nearest neighbor separations required by MCT is still safely less than the mean water spacing, which is of the order 20 Å when D = 67.2 Å.

Most importantly, PT predicts that the scattering in the tails of the peaks should fall off in a Lorentzian fashion as in Eq. 7. This contrasts strongly with the slower power law decay of MCT (Eq. 8), which gives rise to a significant fraction of the scattering occurring in the tails. PT cannot account for this scattering in the tails and it therefore underestimates the form factors for the higher orders, as can be seen in the last row of Table 1 and in the comparison of PT and MCT section above.

It may also be emphasized that simple integration of the experimental scattering data underestimates the tail scattering by approximately the same amount as PT. Whereas the signal is small in these tails, the range of q values is five times the range shown in Fig. 3, so that the lost intensity is significant. Even if one were able to measure the intensity throughout this larger range of q, where the number of counts is small and the background is larger than the signal, the form factors $F(q)$ are continuously varying, so that straightforward integration would yield a distorted result (Zhang et al., 1994). However, with a good theory such as MCT, one can reliably extrapolate the tails into this region from the measurable data shown in Figs. 5–7 for the region near the peaks where the form factor is nearly constant.

The present paper provides the basis for obtaining more reliable form factors for disordered and fluctuating L_α phases. In a subsequent paper, these form factors will be used to determine better electron density profiles and to address various structural issues in lipid bilayers.

This research was supported by National Institutes of Health grant GM44976. CHESS is supported by National Science Foundation grant DMR-9311772 and MacCHESS is supported by National Institutes of Health grant RR01646.

REFERENCES

Als-Nielsen, J., J. D. Litster, R. J. Birgeneau, M. Kaplan, C. R. Safinya, A. Lindegaad-Anderson, and S. Mathiesen. 1980. Observation of algebraic decay of positional order in a smectic liquid crystal. *Phys. Rev. B.* 22:312–320.

Blaurock, A. E., and J. C. Nelander. 1976. Disorder in nerve myelin: analysis of the diffuse X-ray scattering. *J. Mol. Biol.* 103:421–431.

Caillé, A. 1972. Physique cristalline: remargues sur la diffusion des rayons X dans les smectiques. *A. C. R. Acad. Sci. Paris.* 274(Série B):891–893.

DeGennes, P. G. 1974. The Physics of Liquid Crystals. Oxford Press, Clarendon. 284–286.

Franks, N. P., and W. R. Lieb. 1979. The structure of lipid bilayers and the effects of general anaesthetics: an X-ray and neutron diffraction study. *J. Mol. Biol.* 133:469–500.

Garbow, B. S., K. E. Hillston, and J. J. More. 1980. User's Guide for MINPACK. Argonne National Laboratory.

Guinier, A. 1963. X-Ray Diffraction. W. H. Freeman and Co., San Francisco. 300 and 304.

Hosemann, R., and S. N. Bagchi. 1962. Direct Analysis of Diffraction by Matter. North-Holland Publishing, Amsterdam.

Janiak, M., D. M. Small, and G. G. Shipley. 1976. Nature of the thermal pretransition of synthetic phospholipids: dimyristoyl and dipalmitoyllecithin. *Biochemistry.* 15:4575–4580.

Kim, J. T., J. Mattai, and G. G. Shipley. 1987. Gel phase polymorphism in ether-linked dihexadecylphosphatidylcholine bilayers. *Biochemistry.* 26: 6599–6603.

McIntosh, T. J., and S. A. Simon. 1986a. Hydration and bilayer deformation: a reevaluation. *Biochemistry.* 25:4058–4066.

McIntosh, T. J., and S. A. Simon. 1986b. Area per molecule and distribution of water in fully hydrated dilauroylphosphatidylethanolamine bilayers. *Biochemistry.* 25:4948–4952.

Nagle, J. F. 1993. Area/lipid of bilayers from NMR. *Biophys. J.* 64: 1476–1481.

Rand, R. P., and V. A. Parsegian. 1989. Hydration forces between phospholipid bilayers. *Biochim. Biophys. Acta.* 988:351–376.

Roux, D., and C. R. Safinya. 1988. A synchrotron x-ray study of competing undulation and electrostatic interlayer interactions in fluid multimembrane lyotropic phases. *J. Phys. France.* 49:307–318.

Schwartz, S., J. E. Cain, E. A. Dratz, and J. K. Blasie. 1975. An analysis of lamellar x-ray diffraction from disordered membrane multilayers with application to data from retinal rod outer segments. *Biophys. J.* 15: 1201–1233.

Thurmond, R. L., S. W. Dodd, and M. F. Brown. 1991. Molecular areas of phospholipids as determined by ^{2}H NMR spectroscopy. *Biophys. J.* 59:108–113.

Torbet, J., and M. H. F. Wilkins. 1976. X-ray diffraction studies of lecithin bilayers. *J. Theor. Biol.* 62:447–458.

Tristram-Nagle, S., R. Zhang, R. M. Suter, C. R. Worthington, W.-J. Sun, and J. F. Nagle. 1993. Measurement of chain tilt angle in fully hydrated bilayers of gel phase lecithins. *Biophys. J.* 64:1097–1109.

Wiener, M. C., R. M. Suter, and J. F. Nagle. 1989. Structure of the fully hydrated gel phase of DPPC. *Biophys. J.* 55:315–325.

Wiener, M. C., and S. H. White. 1991. Fluid bilayer structure determination by the combined use of x-ray and neutron diffraction. I. Fluid bilayer models and the limits of resolution. *Biophys. J.* 59: 162–173.

Worthington, C. R. 1989. The lamellar structure of intact vertebrate retinal photoreceptors: a verification of phases. *Photobiochem. Photobiophys.* 3:43–51.

Worthington, C. R., and G. F. Elliott. 1989. Helical diffraction. I. The paracrystalline helix and disorder analysis. *Acta Cryst.* A45:645–54.

Worthington, C. R., and R. S. Khare. 1978. Structure determination of lipid bilayers. *Biophys. J.* 23:407–425.

Zhang, R., R. M. Suter, and J. F. Nagle. 1994. Theory of the structure factor of lipid bilayers. *Phys. Rev. E.* 50:5047–5060.

Zhang, R., W. Sun, S. Tristram-Nagle, R. L. Headrick, R. M. Suter, and J. F. Nagle. 1995. Critical fluctuations in membranes. *Phys. Rev. Lett.* 74:2832–2835.